The Dynamics of Flame Flicker in Conical Premixed Flames: An Experimental and Numerical Study

I.G. Shepherd, R.K. Cheng, and M.S. Day*

Lawrence Berkeley National Laboratory
1, Cyclotron Road 70-108B
Berkeley, CA 94720, USA

Corresponding Author:

Ian G. Shepherd,

AETD, Environmental Energy Technologies Division,
B70-108a
Lawrence Berkeley National Laboratory
1, Cyclotron Road 70-108B
Berkeley, CA 94720, USA

Fax: (510) 486-7303
Email: igshepherd@lbl.gov

Colloquium: 4. LAMINAR FLAMES

Total length: 5674 words. Word count etc.

Text: 3423
References: 210
Equations: 182
Figures: 1859
- Figure1 - 179
- Figure2 - 195
- Figure3 - 181
- Figure4 - 442
- Figure5 - 219
- Figure6 - 462
- Figure7 - 181

Abstract: 263

Abstract

Flame tip flicker in premixed conical laminar methane/air flames has been investigated using a coupled experimental and numerical approach. A time-dependent, multidimensional, Low Mach number Combustion Simulation (LMCS), an adaptive mesh refinement technique, has been adopted to handle the large range of scales characteristic of buoyantly driven phenomena. These simulations, using a reduced chemical scheme, are compared with experimental measurements made in a 20 mm diameter ring-stabilized flame with an inlet flow of 0.73 m/s and equivalence ratio, ϕ=0.8. Phase-averaged particle image velocimetry (PIV) provided two-dimensional velocity data. The simulations captured the dynamics of the flame tip oscillation with remarkable fidelity. Time and phase-averaged velocity fields, centerline axial velocities and the flame flicker frequency (10.2 Hz) show good agreement between the numerical and experimental results. The flame tip oscillation is caused by a competition between the pressure fields associated with the predominately radial motion of the burnt gases near the flame front and the rotating vortex motion. The phase-averaged velocity data provided an excellent means for following the evolution of the flow field. Because of the very satisfactory agreement between experiment and simulation a more detailed investigation of the flicker process by means of the much more extensive simulation data was performed. Two types of vortex evolution were observed as alternate vortices were entrained leading to regular variations in the maximum flame tip height. As the inlet flow velocity increases these vortex interactions produce progressively more chaotic flame tip motion. This study shows that a powerful numerical technique coupled with sophisticated experimental diagnostics can lead to significantly improved insight into large-scale combustion/buoyant phenomena.

Keywords: Flame flicker, premixed, laminar, simulation, PIV

Introduction:

A large body of experimental data has been collected [1-3] from which it has been able to characterize the flicker frequency of a premixed conical flame tip. This buoyancy-driven oscillation is associated with the Kelvin-Helmholtz instability and the large vortices formed by the buoyant interaction of the hot burnt gases and the cold ambient air. A number of aspects of the flame/buoyancy coupling have been investigated in normal and micro-gravity environments. Durox and co-workers [4] studied the flame flickering frequency as a function of flow velocity, pressure, and gravitational levels and Kostiuk and Cheng [2] have shown that the flame oscillations have characteristic frequencies (~ 10 - 20 Hz) that can be correlated to a wide range of system parameters. Gotoda et al. [5] have also demonstrated the continued importance of these motions under swirling conditions. These studies have used relatively straightforward diagnostics (such as Schlieren) and analysis; in this work we will elucidate this flame/buoyancy coupling in more detail by using a joint numerical and experimental approach. Simulations using an adaptive, time-dependent, multidimensional, Low Mach number Combustion Simulation (LMCS), benchmarked against a range of two dimensional laboratory experiments, including planar v-flames and axisymmetric non-premixed jet flames [7], are compared to experiments conducted in premixed methane/air laminar flames stabilized on a well-characterized burner [1]

Numerical Methodology:

To investigate buoyancy-driven effects in premixed flames such as flame tip flicker a numerical methodology must accommodate the large difference between the length scales that characterize the combustion zone and those of the buoyant interactions. The preheat zone of a typical premixed methane/air flame front is of the order of 1 mm compared to the vortices generated at the interface between the burnt gas and the ambient air that are of the order of centimeters across and the experimental domains can be 50 or more centimeters long.

This large disparity in scales is accommodated with an adaptive mesh refinement (AMR) technique that maintains a hierarchy of nested rectangular grid patches with levels of increasing refinement. The coarsest level covers the entire domain, and fine patches are created to evolve with small-scale flow and scalar features of interest. The fine grids are nested in successively coarser grids and the system is refined locally until the features of interest are adequately resolved. Local grid patches are destroyed when a coarser representation will suffice. The advantage of this technique, therefore, is that it is capable of modeling large physical domains without sacrificing numerical resolution where it is necessary, in this case to resolve the flame front.

The computational methodology incorporates the variable-density projection formalism in the context of a locally adapting time-dependent hierarchical grid. The code has been implemented in axisymmetric coordinate system and is capable of incorporating arbitrarily complex chemistry, transport and thermodynamic specifications.

A brief outline of the numerical approach follows. This approach treats the fluid as a mixture of perfect gases ignores Soret and Dufort effects and radiative heat transfer and uses a mixture-average model for species diffusion [6]. The familiar equations of momentum transport and conservation of species and enthalpy are:

$$\rho \frac{DU}{Dt} = -\nabla \pi + \nabla \cdot \tau + \rho \vec{g} \tag{1}$$

$$\frac{\partial \rho Y_m}{\partial t} + \nabla \cdot U \rho Y_m = \nabla \cdot \rho D_m \nabla Y_m + \dot{\omega}_m \tag{2}$$

$$\frac{\partial \rho h}{\partial t} + \nabla \cdot U \rho h = \nabla \cdot \lambda \nabla T + \sum_m \nabla \cdot \rho h_m (T) D_m \nabla Y_m \tag{3}$$

where ρ is the density, U is the velocity, Y_m the mass fraction of species m, h the enthalpy of the mixture, g the gravitational acceleration and T the temperature. The production rate of ρY_m, $\dot{\omega}_m$, is obtained from the CHEMKIN-III [7] database. The stress tensor, τ, D_m and λ the diffusion coefficients and thermal conductivity respectively are defined in the normal way. The conservation equations are supplemented by the equation of state for a perfect gas mixture, where R is the universal gas constant,

$$p_0 = \rho R_{mix} T = \rho R T \sum_m \frac{Y_m}{W_m} \tag{4}$$

and a relationship between enthalpy, species and temperature

$$h = \sum_m Y_m h_m (T) \tag{5}$$

In the low Mach number model, the equation of state constrains the evolution and removes acoustic wave propagation from the dynamics.

The basic discretization combines a symmetric operator-split coupling of chemistry and diffusion processes with a density-weighted approximate projection method. The projection method imposes a constraint on the velocity divergence that forces the evolution to satisfy the equation of state. The resulting integration of the advective terms proceeds on the time scale of the relatively slow advective transport. Faster diffusion and chemistry processes are treated time-implicitly. This integration scheme is embedded in a parallel adaptive mesh refinement algorithm framework based on a hierarchical system of rectangular grid patches. The complete integration algorithm is second-order accurate in space and time, and discretely conserves species mass and enthalpy. The reader is referred to for Details of the low Mach number model and its numerical implementation may be found in [9] and its application to the simulation of premixed turbulent flames in [8].

Experimental Details:

The experiments were performed in a flame stabilized on a burner with a 25*mm* diameter circular outlet supplied by a converging nozzle fitted to a cylindrical settling chamber. The converging nozzle produces laminar flow with a uniform velocity distribution. Conical flames are stabilized by a ring fitted inside the rim (1) that reduces the effective diameter of the burner outlet to 20.6 *mm*. Its purpose is to stabilize premixed flames at lean stoichiometries.

Two-dimensional, radial and axial velocity data are obtained with a Particle Imaging Velocimetry (PIV) system that consists of a New Wave Solo PIV YAG laser with double 120 mJ pulses at 532 *nm* and a Kodak/Red Lake ES 4.0 digital camera with 2048 by 2048 pixel resolution. The repetition rate of the laser, however, is restricted to 10 Hz, a sampling frequency too low to time resolve the flame tip frequencies (>10 Hz). Phase-locked flowfield information is, therefore, obtained by triggered the PIV system using a Schlieren-based flame motion sensor previously used for measuring the flame fluctuation frequencies [1]. The optics are configured to capture a field of view of approximately 130 *mm* by 130 *mm* covering the near field (i.e. the flame zone) as well as the far field of the flames with a 0.065 mm/pixel resolution. A cyclone type particle seeder seeded the air flow with 0.5 μm Al_2O_3 particles. Data acquisition and analysis were performed using software developed by Wernet [10]. Care was taken to optimize interframe timing (120 μs), camera aperture setting, laser-sheet thickness, and seed density to ensure high data fidelity.

The flame motion sensor consists of a He-Ne laser beam that traverses the flame tip and is focused on a Schlieren stop. A photo diode placed behind the Schlieren stop produces an AC signal that shows the cyclic variations in the flame tip motion. From inspection of this signal the frequency of the flame tip motion can be determined. The positive-going zero crossing of this signal was used as the reference point from which different phase-angles of the flame fluctuation cycles can be captured by varying the time-delay at which the laser was fired. By this means it is possible to condition the data collection and obtain data at specific phase angles. For each flame, mean velocity vectors are obtained at four phase angles (0^o, 90^o, 180^o and 270^o) by recording and averaging a set of 100

image-pairs. The PIV data are processed using 32x64 pixel cross-correlation interrogation regions with 50% overlap giving a spatial resolution of ~1 *mm*. The velocity statistics are checked to ensure that significant spatial bias or "peak-locking" was not taking place.

Results and Discussion:

Two dimensional, axisymmetric simulations of premixed stoichiometric laminar methane/air conical flames were performed with a reduced chemistry two-step, six species reaction scheme with the species O_2, H_2O, CH_4, CO, CO_2, and N_2:

$$2CH_4 + 3O_2 = 2CO + 4H_2O$$

$$2CO + O_2 = 2CO_2$$

The reaction rates were chosen so that the laminar burning rate, S_L, for an equivalence ratio, $\phi = 0.9$ mixture was matched with tabulated values. Two variables, S_L and the unburnt/burnt gas density ratio, ρ_u/ρ_b, where subscripts *u* and *b* refer to unburnt and burnt conditions, are of primary importance in controlling the flame dynamics and the buoyant interactions. This can be seen by considering the Richardson number, *Ri*, which is the ratio of buoyant to inertial forces:

$$Ri = g\left(\frac{\rho_u}{\rho_b} - 1\right)\frac{d_b}{S_b^2} \qquad (6)$$

where d_b is the burner diameter and S_b is the laminar burning velocity relative to the burnt gas system. It was concluded therefore that a more realistic reaction mechanism was not necessary at this stage where an understanding of overall flame dynamics and mechanisms is being sought. It should be emphasized that the simulations are not 'tuned' to fit the experimental results

A range of cases are measured and simulated for premixed methane/air flames over an inlet velocity range of 0.73 *m/s* to 1.53 *m/s* and stoichiometeries from ϕ=0.8-1.0. In this paper only results from the lowest velocity case (ϕ=0.8) are presented due to space limitations and because under these conditions the flicker frequency is highly regular (see figure 3) and so consequently the phase-averaging necessary to obtain the experimental data are most robust. This case therefore provides the best conditions for comparing experimental and simulation results.

Figure 1 compares an experimental PIV image and a snapshot of the simulated density field. The PIV image shows half the experimental domain (40*140 *mm*). The region of heavier seeding at the bottom of the image is the reactant zone upstream of the flame front. In the simulation image (at a similar point in the flicker cycle) a centerline symmetry condition is assumed in the calculation computational domain size being 320x640 *mm*. This large computational domain was adopted to reduce boundary effects and to accommodate the long-range buoyant interactions. In the simulation the flame is rim stabilized and as it does not include the ring stabilizer used in the experimental

burner the base is larger (r=12.9 mm) than in the experiment (r=10 mm). This leads to the higher flame heights in the simulations, see figure 5. Given the simplicity of the chemical reaction used here no detailed attempt was made to match the laminar flame velocity to that of the experiment. Although the burning velocity appears to be a little lower in the simulations, the similar flame angles indicate that the burning velocities are also similar.

The time averaged velocity vectors for PIV, from 224 random image-pairs and LMCS are compared in figure 2 where r is the radial and z the axial components and V and W the respective velocities. The simulation is averaged over 1.27 secs: more than 12 complete cycles. The time step was 6.7 x 10^{-4}*s* and data was saved every 10 time steps i.e. 191 data sets were averaged. Data from the lowest inlet flow velocity (W_o = 0.73 *m/s*, ϕ=0.8) is presented in this paper for the reasons discussed above. At higher velocities it is apparent that the flame flickering becomes progressively more chaotic: this aspect is currently under investigation. To highlight the vector length the W/V vectors are colored by their magnitude $W_{mag} = (W^2+V^2)^{0.5}$. The experimental and simulation results are very similar and the picture that emerges from these time-averaged data is familiar. The high flame angle causes most of the initial gas to accelerate in the radial direction and then buoyant acceleration and interaction with stagnant outer air deflects the flow upward. As discussed above it is well known that this picture does not represent the detailed dynamics of the buoyant laminar flame/flow interactions.

As mentioned earlier flame tip flickering has been well characterized experimentally and its cause traced to buoyantly accelerated vortices that form at the unstable interface between the high velocity hot products and the surrounding still, cold see figure 3. The data in figure 3 was obtained from the simulations, the inset showing the variation of flame tip height with time. The flame tip position in the simulations was determined from centerline profiles of the density and defined to be the point of maximum density gradient in the flame zone. The normalized flame height, h*=h/<h> shows that the peak-to-peak oscillation amplitude is approximately 10% of the mean height. The flame tip oscillation is very regular the spectrum, figure 3, has a dominant frequency at 10.2 Hz. The experimental value obtained for this condition was 11.7 Hz [???] a difference primarily due to the different burner sizes. Also observable in the time history and spectrum is a~5 Hz sub-harmonic; every alternate vortex generates a slightly larger flame tip excursion due to vortex entrainment. This phenomenon is discussed in detail below.

The regularity of this frequency, especially in this low velocity case, make it is possible to compare experimental and simulation data by phase averaging and an averaged time history of the flame vortex interaction can be obtained. Data were collected at phase angles of 0^o, 90^o, 180^o and 270^o where 0^o refers to the maximum flame tip height. In figure 4 the phase averaged velocity vector data obtained from the experiment and the simulation are directly compared, the same vector coloring being used as in figure 2. The simulation recovers all the features observed by the experiment. Lines in the simulation results (unavailable from the experiments) are density iso-contours: ρ=0.9, (dashed line) characterizes the initial mixing between the cold outer air and the combustion products

and ρ=0.4 (solid line) delineates the high velocity region. Between these two contours the buoyancy-driven vortices form; a cross marks the center of rotation of the vortices. The mean flame front position at each phase angle appears in the bottom left hand corner of each figure where these contours are very close together.

The vortex 'pumping' mechanism process may be summarized as follows. The heat release at the flame front forces the burnt gas flow predominantly in the radial direction (see figure 2) but the pressure field associated with the rotating vortex motion opposes this flow. It is the competition between these two phenomena that causes the flame to flicker. Examination of figure 4 clearly demonstrates this process. At θ=270^o the formation of a vortex may be observed at the kink in the ρ=0.4 contour at *r*=20 *mm* and *z*=30 *mm* (see figure 6 for more detail). The affect of rotating vortex motion on the burnt gases is at a maximum at θ=0^o causing the higher temperature region, ρ<0.4, to narrow. At this point the flame height is at a maximum. As the vortex is convected downstream away from the flame (see the position of the black crosses), its effect lessens and the burnt gas region close to the flame broadens, see the ρ=0.4 contour, the flame height falls to a minimum at θ=180^o and a large low velocity region just downstream has formed. With the formation of a new vortex at θ=270^o the cycle repeats.

The affect of this interaction is clearly discernable in Figure 5 that compares the experimental and numerical values for the phase-averaged axial centerline velocity. Heat release at the flame front causes the sudden velocity increase at *z*~20 mm (experiment) and *z*~37 mm (simulation). As mentioned above the differing mean flame heights derive

from the larger burner base and lower burning velocity in the simulations. The profiles as a function of phase angle are in excellent agreement showing that the simulation has captured the essential features of this unstable phenomenon. The large rise in the axial velocity just downstream of the flame front in the first quarter of the cycle ($\theta=0^o$ to $\theta=90^o$) and subsequent decline at $\theta=180^o$ where the flame height is at a minimum are clearly observed in both the experiment and simulation.

A more detailed picture of the flame/vortex interaction can be obtained the simulations. Figure 6 shows time history of the density field over three cycles. The white box in the first frame indicates the half-width size of the experimental domain; the simulation images illustrate only approximately 50% of the entire computational domain. Plotted beneath the images is the normalized flame height obtained from these images. The images are sequential instantaneous snapshots at the four phase angles used for the phase-averaged data in figure 4 and show the formation, between $\theta=270^o$ and $\theta=0^o$ of a vortex and its subsequent time history. Two characteristic vortex evolutions are found: a) from T=0 to T=0.1 where the vortex is convected downstream and survives to the end of the computational domain and (b) from T=0.1 to T=0.2 where the vortex is entrained by the previous vortex that causes the maximum flame height to be higher than in the case without entrainment. This effect is also observed in the inset in figure 2 and the sub-harmonic in the power spectrum. This result indicates that the flame flickering is controlled by both these vortices, a process not clear from the experimental data.

The differing behavior of the two types of vortex may be readily illustrated by considering their downstream evolution. Figure 7 shows the vortex convection speeds,

V_c, as functions of downstream distance and time (the inset). The convection speeds were obtained from plots of the trajectories of the vortex centers of rotation in *rz* space. The unentrained vortices, as might be expected, experience buoyant acceleration throughout the domain and at the end of the domain have reached velocities from 1-1.5 m/s which may be compared with centerline velocities of approximately 3 m/s (figure 5) with a constant acceleration of 1.28 m/s^2. The time history of the convection speed in the inset shows that the acceleration is constant throughout the domain (dashed line).

The entrained vortices, as is clear in figure 6, have a quite different behavior. The inset in Figure 7 shows (solid line) that after an initial deceleration, the vortex, under the influence of the velocity field of the previous vortex, is rapidly accelerated (up to 80 m/s^2) and entrained into the main burnt gas flow near the centerline. At this point, z/D = 4.5 and T=0.475 *s* it is no longer possible to locate a center of rotation for the vortex. A vortex formed after one that has been entrained cannot be similarly entrained and so this process occurs every other vortex, producing the alternating pattern in flame height observed in figures 3 and 6. It is interesting to note that this entrainment process does not alter the flicker frequency and seems to have little effect on the convection of the original vortex, see figure 7 (inset). It is clear, however, that the flame tip dynamics are also controlled by the interaction between the vortices. As the inlet flow velocity is increased such interactions become much more significant and the flickering of the flame tip becomes progressively more chaotic. Due to the experimental difficulties mentioned earlier and the limitation in space this data could not be presented here but an investigation of this phenomenon continues.

Conclusions:

Flame tip flicker in premixed conical laminar flames has been investigated using a coupled experimental and numerical approach. An adaptive mesh refinement technique has been adopted to deal with the large range of scales characteristic of buoyantly driven phenomena: a time-dependent, multidimensional, Low Mach number Combustion Simulation (LMCS) with a simple chemical scheme. The results from these simulations are compared with experimental measurements that employed phase-averaged particle image velocimetry which provides the two-dimensional velocity data. This experimental approach was necessary because of the low laser repetition rate and made possible by the very regular flame oscillations at the low inlet velocity conditions selected for these comparisons.

The simulations captured the dynamics of the flame tip oscillation with remarkable fidelity. Time and phase-averaged velocity fields, centerline axial velocities and flame flicker frequency show good agreement between the numerical and experimental results.

Buoyantly accelerated vortices form at the unstable interface between the hot product gases and the cold ambient air. The vortex 'pumping' phenomenon which causes the flame tip oscillation is a competition between the pressure fields associated with the predominately radial motion of the burnt gases near the flame front and the rotating flow of the vortex. The development of the flow field under the influence of these forces can be clearly discerned from the phase-averaged velocity data.

The very satisfactory agreement between experiment and simulation encouraged a more detailed investigation of the flicker process by means of the much more extensive data available from the simulation. Two types of vortex evolution were observed as alternate vortices were entrained leading to regular variations in the maximum flame tip height. As the inlet flow velocity is increases preliminary analysis reveals that these vortex interactions produce progressively more chaotic flame tip motion.

This study demonstrates that the coupling of a powerful numerical technique with sophisticated experimental diagnostics can lead to significantly improved insight into large scale combustion/buoyant phenomena.

Ackowledgements:

This work was supported by the Nasa Microgravity Program and monitored by Dr. Paul Greenberg. MD had additional support from the Office of Science through the Office of Advanced Scientific Computing Research, Mathematical, Information, and Computational Sciences. The authors are very grateful to Dr. Hiroshi Gotoda for his help in data reduction.

References:

[1] Kostiuk, LW., and Cheng, R.K., *Experiments in Fluids*, Vol. 18, pp. 59 - 68, 1994.

[2] Kostiuk, LW., and Cheng, RK., *Combust. and Flame*, vol. 103, pp. 27 - 40, 1995.

[3] Bedat, B. and Cheng, R.K., *Combust. and Flame* 107:13 (1996).

[4] Durox, D., Baillot, F., Scoufflaire, P., and Prud'homme, R., *Combust. and Flame*, Vol. 82, pp. 66 - 74, 1990.

[5] Gotoda, H., Maeda, K., Ueda, T., and Cheng, R.K., *Combust. and Flame*, vol. 134, pp 67 - 79, 2003.

[6] Warnatz, J., *Numerical methods in flame propagation*, eds N. Peters and J. Warnatz, Friedr. Viewweg and Sohn, Wiesbaden, (1982).

[7] R. J. Kee, J. F. Grcar, J. A. Miller, E. Meeks, and M. Smooke. *PREMIX Users Manual*. Reaction Design, San Diego, CA, (1998).

[8] J. B. Bell, M. S. Day, J. F. Grcar, *Proc. Combust. Inst*. 29 (2002) 1987–1993.

[9] M. S. Day, J. B. Bell, *Combust. Theory Modelling* 4 (2000) 535–556.

[10] M.P. Wernet Fuzzy Logic Enhanced Digital PIV Processing Software, *18th International Congress on Instrumnetation for use in Aerospace Simulation Facilities (ICIASF)*, Toulouse, France, June 1999.

List of Figures:

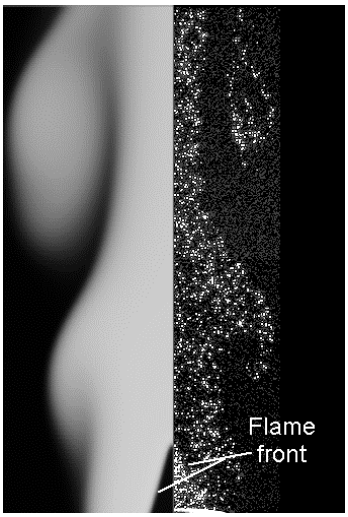

Figure 1: Comparison of instantaneous PIV image and LMCS density field

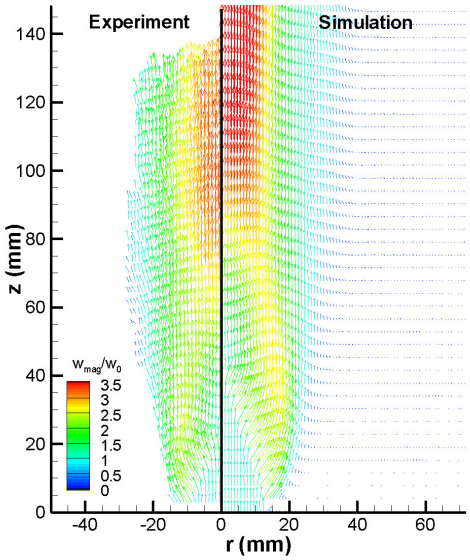

Figure 2: Comparison of time averaged experimental and simulation velocities

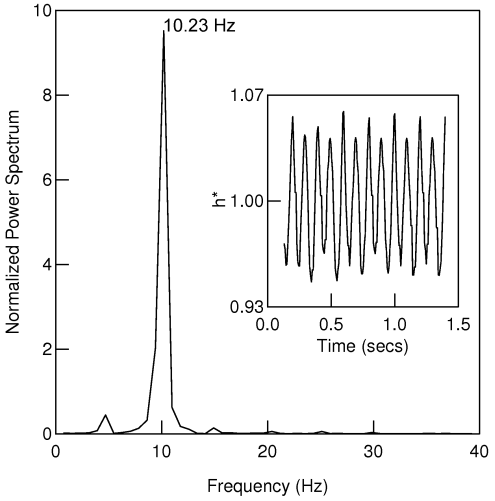

Figure 3: Power spectrum and time history (inset) of normalized flame tip height, h* (simulation)

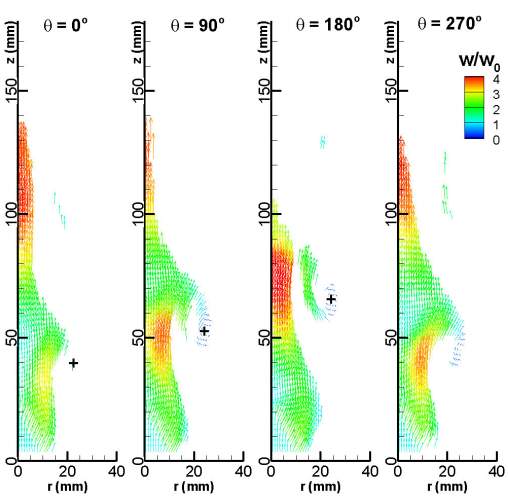

Figure 4a: Phase averaged PIV data. The black crosses are at the vortex centers.

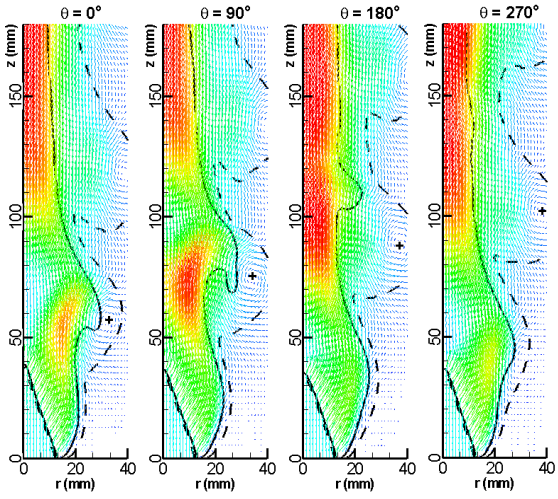

Figure 4b: Phase averaged LMCS. The lines are iso-contours of density, ρ=0.9 (dashed), ρ=0.4 (solid). The black crosses are at the vortex centers.

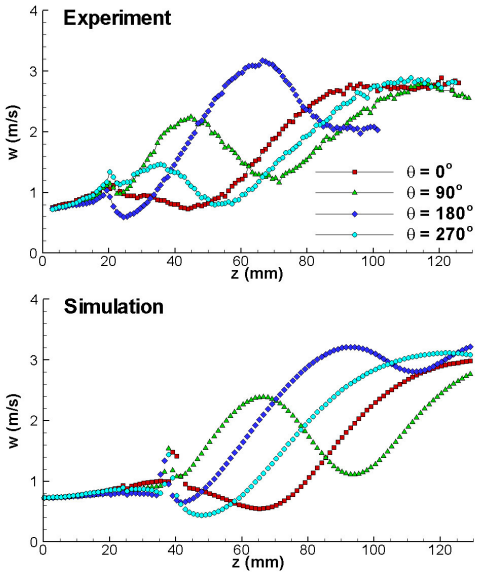

Figure 5: Average axial centerline velocity as a function of phase angle

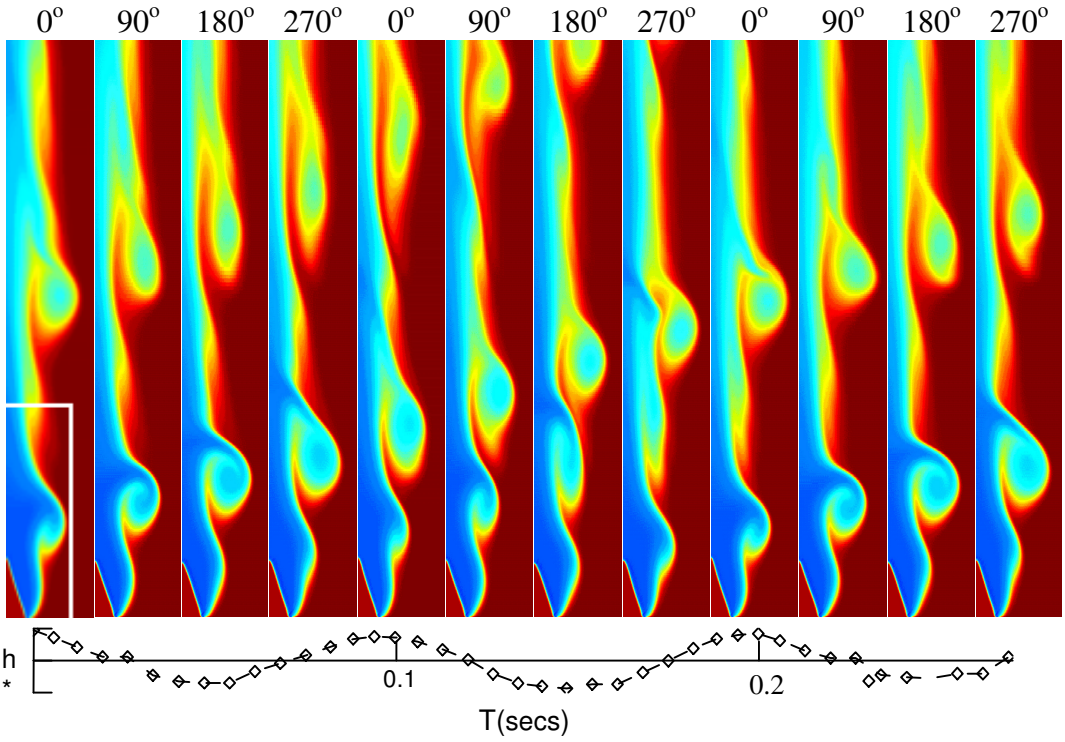

Figure 6: Time evolution of density field showing vortex entrainment phenomenon. The flame height is shown underneath. White box in first frame shows experimental domain.

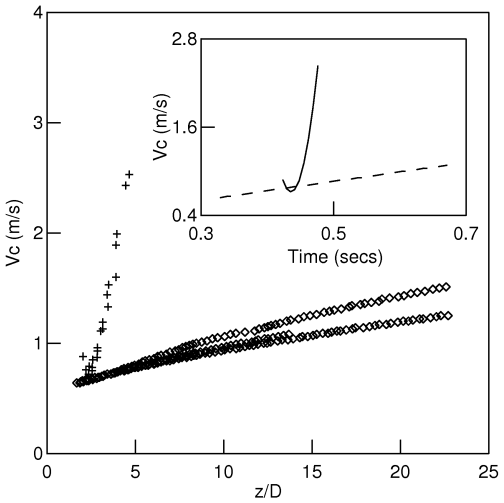

Figure 7: Convection speed of vortices, V_c as a function of downstream distance. Inset shows acceleration of vortices.